One Dimensional Arrays and Solitary Tunnel Junctions in the Weak Coulomb Blockade Regime: CBT Thermometry

Sh. Farhangfar, K. P. Hirvi, J. P. Kauppinen, J. P. Pekola, and J. J. Toppari

Department of Physics, University of Jyväskylä, P.O. Box 35, 40351 Jyväskylä, Finland

D. V. Averin

Department of Physics, SUNY, Stony Brook, New York 11794, USA

and

A. N. Korotkov

Nuclear Physics institute, Moscow State University, Moscow 119899, Russia

(Received December 12, 1996; revised February 11, 1997)

In this article we review the use of the tunnel junction arrays for primary thermometry. In addition to our basic experimental and theoretical results we stress the insensitivity of this method to the fluctuating background charges, to nonidealities in the array and to magnetic field. Important new results of this article are the low temperature corrections to the half width and depth of the measured conductance dip beyond the linear approximation. We also point ou that short arrays, single tunnel junctions in particular, show interesting deviations from the universal behaviour of the long arrays.

1. INTRODUCTION

Single electron tunnelling (SET) effects have been intensively studied for the past few years.[1] The properties of SET components, in particular of 1D arrays, in the low temperature regime, $k_B T \ll E_c$, where E_c is the charging energy of the system, have been widely discussed,[2,3] whereas the opposite limit $k_B T \gg E_c$ has been largely overlooked. Yet one dimensional arrays of normal metal tunnel junctions exhibit properties which are very suitable for primary and secondary thermometry in a lithographically adjustable temperature range which extends over two decades in the $k_B T > E_c$ regime.

The thermometer is remarkably insensitive to nonuniformities in the actual pattern and to even strong magnetic fields. We discuss the behaviour of this device at low temperatures where the hot electron effect due to poor electron phonon coupling ultimately takes over at $T \ll 1$ K, and at high temperatures, $T \gg 50$ K, where the barrier suppression limits the use of AlOx based junctions. Short arrays, and especially single tunnel junctions show interesting deviations from the universal behaviour of the long array. Our work on tunnel junctions in the weak Coulomb blockade regime is mostly based on the orthodox theory of tunnelling of Ref. 1, and it has been reported in Refs. 4, 5, 6, 7, and 8.

2. THEORY OF CHARGING EFFECTS IN THE HIGH TEMPERATURE LIMIT

A. The First Order Results for Weak Coulomb Blockade

We start with a brief theoretical description of a 1D array of N normal metal tunnel junctions, which is schematically shown in Fig. 1. The resistance of the ith junction is denoted by $R_{T,i}$, and its capacitance by C_i. The stray (ground) capacitance of the ith island, between the ith and $(i + 1)$th junctions, is $C_{0,i}$. In general, we may allow non-equal values for $R_{T,i}$, C_i, and $C_{0,i}$ at different i, i.e., inhomogenities in the array, biased at $\pm V/2$ at its ends.

Simple formulae for the IV-curve and its easily measurable derivative, i.e., the differential conductance, G, in the case of an arbitrary N-junction array were obtained in Ref. 5 with a result

$$G/G_T = 1 - 2 \sum_{i=1}^{N} \frac{R_{T,i}}{R_\Sigma} \frac{\Delta_i}{k_B T} g\left(\frac{R_{T,i}}{E_\Sigma} eV/k_B T\right) \tag{1}$$

using a high temperature expansion with $\Delta_i \ll k_B T$ up to the first order. Δ_i, the Coulomb blockade threshold for the ith junction, originates from the
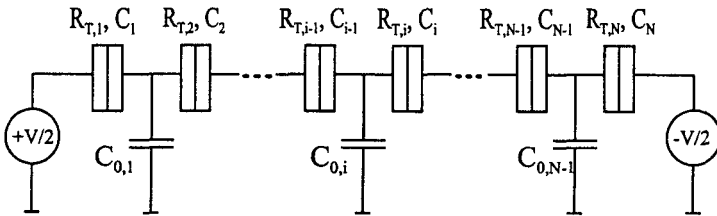

Fig. 1. A one dimensional tunnel junction array. The divided rectangles represent normal metal based junctions.

inverse capacitance matrix, $\mathbf{C}^{-1}$, of the array[5]: $\Delta_i = (\mathbf{C}^{-1}_{i-1,i-1} + \mathbf{C}^{-1}_{i,i} - 2\mathbf{C}^{-1}_{i,i-1})e^2/2$. The function g was introduced in Ref. 4 and defined by

$$g(x) = [x \sinh(x) - 4 \sinh^2(x/2)]/8 \sinh^4(x/2) \qquad (2)$$

and we denote the total tunnel resistance by R_Σ, i.e., $R_\Sigma \equiv \sum_{i=1}^{N} R_{T,i}$. G_T is the asymptotic value of G when $V \to \pm \infty$.

In the fully symmetric case with $R_{T,i} \equiv R_T$, $C_i \equiv C$ and $C_{0,i} \equiv 0$ we obtain

$$G/G_T = 1 - u_N g(v_N) \qquad (3)$$

with $u_N \equiv 2[(N-1)/N](e^2/2C/k_B T)$ and $v_N \equiv eV/Nk_B T$. This represents a nearly bell shaped dip in conductance and the full width at half minimum, $V_{1/2}$, depends only on N and T:

$$V_{1/2} \simeq 5.44 Nk_B T/e \qquad (4)$$

The depth depends on capacitances through u_N as

$$\Delta G/G_T = (1/6)u_N \qquad (5)$$

Equations (4) and (5) are our central results on primary and secondary thermometry, respectively.

B. Higher Order Corrections

Higher order terms in the expansion yield corrections to the results of Eqs. (3–5) of a symmetric array. To obtain these we use a slightly different approach. Instead of calculating the probabilities of different electron configurations on the island, and writing current as a sum of tunnelling rates weighted by these probabilities, we calculate the probabilities of the configurations $\{\tilde{V}_i\}$, where $\tilde{V}_i$ is a fluctuation from the average voltage drop V/N of the ith junction. From these configuration probabilities we then can obtain probabilities for the ith junction to have a fluctuation $\tilde{V}_i$. To find the configuration probabilities σ we need a master equation which can be written for N junctions as

$$\dot{\sigma}(\{n_j\}) = \sum_j \{\sigma(..., n_j - 1, n_{j+1} + 1,...) \, \Gamma_j^-(..., n_j - 1, n_{j+1} + 1,...)$$

$$+ \sigma(..., n_j + 1, n_{j+1} - 1,...) \, \Gamma_j^+(..., n_j + 1, n_{j+1} - 1,...)$$

$$- [\Gamma_j^+(..., n_j, n_{j+1},...) + \Gamma_j^-(..., n_j, n_{j+1},...)] \, \sigma(..., n_j, n_{j+1},...)\} \qquad (6)$$

In steady state we have $\dot{\sigma}(\{n_j\}) = 0$ and Eq. (6) can be written in a linearised approximations as a differential equation

$$\sum_{j=0}^{N-1} \left(\frac{\partial}{\partial n_{j+1}} - \frac{\partial}{\partial n_j} \right) \left[eV_j \sigma(\{n_i\}) + \frac{1}{2} h(v_N) k_B T \left(\frac{\partial}{\partial n_{j+1}} - \frac{\partial}{\partial n_j} \right) \sigma(\{n_i\}) \right] = 0 \tag{7}$$

with $h(x) = x \coth(x/2)$. Here V is the voltage applied over the whole array and V_j is the (fluctuating) voltage drop across the jth junction. Since eV_j can be expressed in terms of the energy of the symmetric array, $W(\{n_j\}) = \sum_{j,k=1}^{N-1} e^2/(2CN) \cdot j(N-k) n_j n_k$, we can solve Eq. (7) and obtain

$$\sigma(\{n_j\}) \propto \exp\left[-\frac{2W(\{n_j\})}{h(v_N) k_B T} \right] \tag{8}$$

Since each occupation configuration $\{n_i\}$ corresponds to a certain voltage configuration $\{V_i\}$ across the junctions in the array, we can make a change of variables from n_i to V_i. Furthermore, we may write each voltage drop as $V_i = V/N + \tilde{V}_i$. Making use of the fact that $W(\{\tilde{V}_i\}) = (C/2) \sum_k \tilde{V}_k^2$ we can express probabilities $\sigma(\{n_i\})$ using $\{\tilde{V}_i\}$:s. The probability for the ith junction to have a fluctuation $\tilde{V}_i$, $\sigma(\tilde{V}_i)$, can then be calculated using these. After normalization, i.e., by setting $\int_{-\infty}^{\infty} \sigma(\tilde{v}_i)\, d\tilde{v}_i = k_B T/e$ with $\tilde{v}_i = e\tilde{V}_i/k_B T$, we finally obtain

$$\sigma(\tilde{v}_i) = \frac{e}{k_B T} \sqrt{\frac{1}{u_N \pi h(v_N)}} \exp\left[-\frac{\tilde{v}_i^2}{u_N h(v_N)} \right] \tag{9}$$

Note that we assume $\tilde{v}_i$ to be a continuous variable.

We can write the current as

$$I = k_B T \int_{-\infty}^{\infty} \sigma(\tilde{v}_i) [\Gamma_i^+(v_N, \tilde{v}_i) - \Gamma_i^-(v_N, \tilde{v}_i)]\, d\tilde{v}_i \tag{10}$$

where the tunnelling rates forwards and backwards in the ith junction, $\Gamma_i^\pm(v_N, \tilde{v}_i)$, can be obtained from the change of the free energy, $\Delta F_i^\pm$, in the corresponding tunnelling event.[4] Thus one obtains for the two tunnelling rates, e.g., in the first junction

$$\Gamma_1^\pm = \frac{k_B T}{e^2 R_T} \cdot \frac{\pm v_N \pm \tilde{v}_1 - u_N/2}{1 - \exp[\mp v_N \mp \tilde{v}_1 + u_N/2]} \tag{11}$$

Using the high temperature expansion with $u_N \ll 1$ we obtain the same first order result as in Eq. (3), but now we can proceed to higher order corrections as well:

$$G/G_T = 1 - u_N g(v_N) - \tfrac{1}{4} u_N^2 [\, g''(v_N)\, h(v_N) + g'(v_N)\, h'(v_N)\,]$$

$$- \tfrac{1}{8} u_N^3 [\, \tfrac{1}{4} g''''(v_N)\, h(v_N)^2 + \tfrac{1}{3} g''(v_N) + \tfrac{1}{2} g'''(v_N)\, h'(v_N)\, h(v_N)\,] - \dots \tag{12}$$

From this we can obtain the linear correction to the full width at half minimum in Eq. (4):

$$\frac{\Delta V_{1/2}}{V_{1/2,0}} \simeq 0.39211 \frac{\Delta G}{G_T} \tag{13}$$

where $V_{1/2,0}$ is full width at half minimum from Eq. (4) and the numerical factor 0.39211 originates from the functions h, g and their derivates at $v_N = (1/2)(eV_{1/2,0}/k_B T)$. In the same way we obtain corrections to the depth of the conductance curve beyond Eq. (5):

$$\Delta G/G_T = (1/6)u_N - (1/60)u_N^2 + (1/630)u_N^2 + \dots \tag{14}$$

The effect of these corrections is to flatten and to broaden the conductance dip.

To check the validity of the analytic method, and to investigate the effect of non-zero background charges (See Ch. 2C), we also performed stochastic Monte-Carlo (MC) calculations.[6] This basic method could, however, be accelerated significantly at higher temperatures over the method used, e.g., in Ref. 9, by a "hybrid" like method, where just the charge configuration is obtained by means of MC, but the current through the array is calculated as a sum of tunnelling rates weighted by the corresponding probabilities of configurations. The linear correction to the full width at half minimum obtained by this method agrees well with the analytic correction (13) as shown in Fig. 2.

C. Nonidealities of the Arrays

Equation (1) yields a quadratic dependence for $V_{1/2}$ in the case of small variations in junction parameters such that

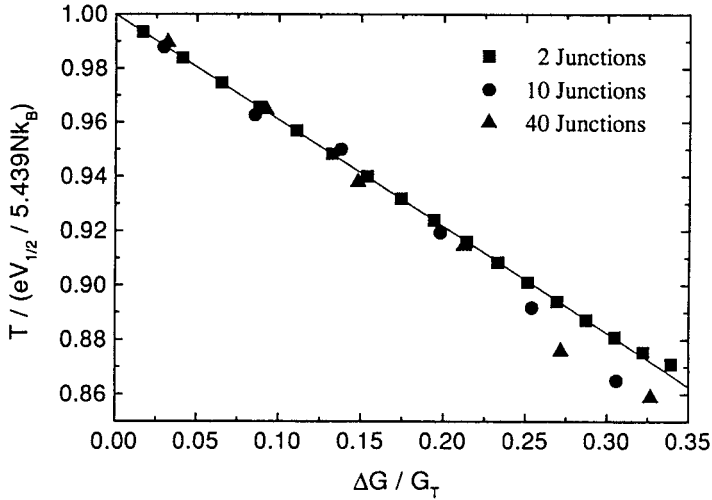$$V_{1/2}/(5.44Nk_B T/e) \simeq 1 - k[\delta R/R_0]_{rms}^2 \tag{15}$$

Fig. 2. Low temperature corrections to temperature obtained from Eq. 4. The solid line is from Eq. (13) and the data points are obtained by the Monte Carlo-method of Ref. 6.

where $[\delta R/R_0]_{rms}$ is the rms deviation of the junction resistances from their mean value $R_0 \equiv R_\Sigma/N$ in the array, and we have made the natural assumption that $R_{T,i} C_i = constant$ throughout the array (see Sec. 4C). The numerical factor k has a value $k \simeq 0.73 + (N-1)/N$.

In calculations above we assumed that the ends of an array were ideally biased at $\pm V/2$, i.e., the potentials at the ends did not change due to tunnelling. In practice this is not true. When electron tunnels through the first or the last junction to or from the end of the array it changes the potential in there. This voltage fluctuation then recovers within a time determined by the impedance of the environment, i.e., the connecting wires and capacitances. This is the reason for the observed charging peaks on single junctions discussed in Sec. 5. In an array with large N the effect due to its ends is negligible compared to the charging effects of the $N-1$ islands.

A technically more complicated problem is that of the background charges in the array. Those are highly uncontrollable in the experiment and produce nonidealities to the charging effects. To find out the influence of the background charges we used the Monte Carlo-method mentioned earlier.[6] In these simulation runs we introduced on each island a random offsett charge $q_{0,i}$ drawn from a uniform distribution within the interval $[-e/2, +e/2]$ since the effect of $q_{0,i}$ is e periodic. The uniform distribution reflects that fact that no particular configuration of $q_{0,i}$ is preferred in experiment. Some runs were performed with uniform nonzero background
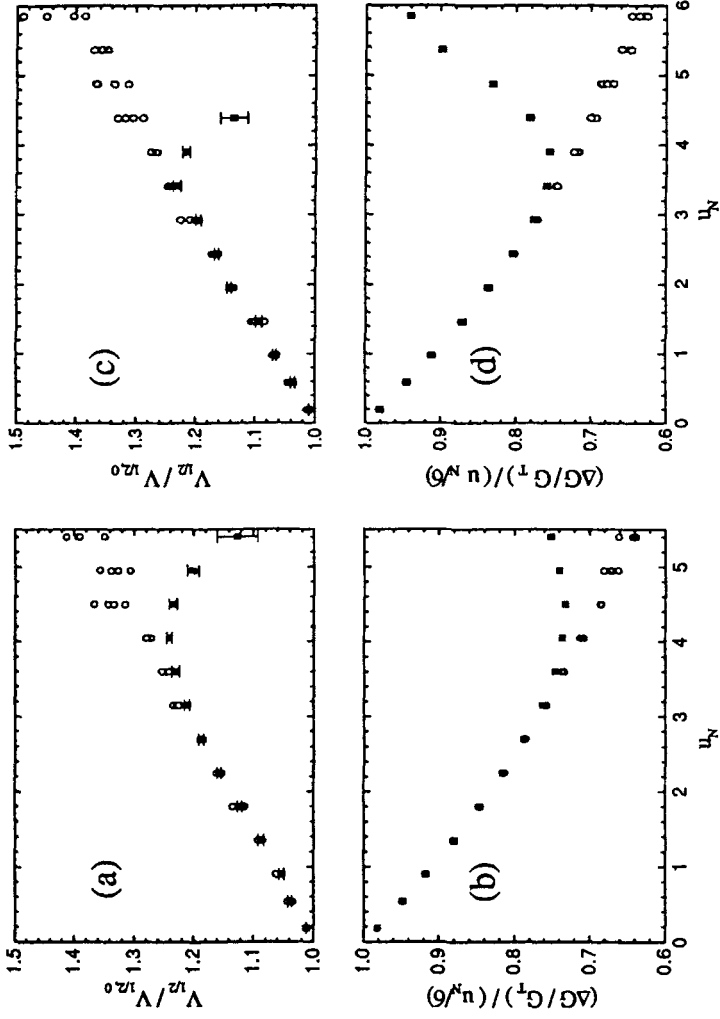
Fig. 3. Background charge effects on $V_{1,2}$ and $\Delta G/G_T$ for symmetric 10 (a), (b) and 40 (c), (d) junction arrays vs. u_N. Each point in the figure was calculated with a different set of background charges (circles) $\{q_{0,i}\}$. The homogeneous case ($q_{0,i} = 0$) is plotted with solid square symbols.

charges with results equal to those in any other configurations in high temperature regime.

The effect of the background charges on $V_{1/2}$ and the dip height are shown in Fig. 3 for 10 and 40 junction arrays. The two junction case was studied in Ref. 4. It is seen from Fig. 3 that correction to the analytic first order half width, $V_{1/2,0}$ obtained from Eq. (4), is linear at high T and that background charges do not affect $V_{1/2}$ and $\Delta G/G_T$ until $u_N \simeq 3$. The two junction case starts to show sensitivity to background charges from $u_N \simeq 2$ upwards.[4] A qualitative explanation for this insensitivity to background charges at higher temperatures originates from the temperature dependence of the probabilities $\sigma(\{n_i\})$. The probability of configurations with n_i electrons on a particular island, $\sigma(n_i) = \sum_{n_j, j \neq i} \sigma(n_1, n_2,..., n_i,..., n_{N-1})$, is peaked around $n_i = 0$ and normally distributed. The square of the width of this gaussian distribution is lineary dependent on temperature. Obviously, background charges $q_{0,i}$ start to have a noticeable effect only when the spread in charge drops down to that of $q_{0,i}$'s, i.e., at low temperatures.

3. FABRICATION OF THE SENSORS AND EXPERIMENTAL TECHNIQUES

We fabricate samples by electron beam lithography and standard shadow evaporation of aluminium on oxidized silicon substrates. The tunnel barrier is formed in pure oxygen at room temperature. Figure 4 shows thermometers (a) for low temperatures with large junctions and islands and with cooling fins attached, and (b) for high temperatures with ultra small junctions and islands, respectively. In the experiments we have investigated samples with capacitances ranging from $C_\Sigma = 0.2$ fF up to $C_\Sigma = 15$ fF. The areas of the tunnel junctions are varied in the range $6 \times 10^{-3} - 1.5$ $(\mu m)^2$. The resistances are on the order of 100 kΩ.

For cross checking the CBT thermometers we employ calibrated Cernox resistors from Lake Shore, superconducting transition temperatures at zero magnetic field of pure Pb at 7.19 K, Al at 1.18 K, and Ti at 0.39 K, and 4.215 K of boiling ^{4}He at 760 mmHg, and most recently 77 K of boiling N$_2$ at 760 mmHg. The conductance vs. bias voltage has been measured with a linear DC voltage sweep typically in ~ 3 minutes across the full bias range with a sufficiently low amplitude AC modulation ($V_{AC} \ll V_{1/2}$) typically at 10 Hz. Very recently a prototype of a compact measuring bridge for CBT-thermometers has been constructed. Measurements are carried out either in our home made plastic dilution refrigerators[10] down to 50 mK, or inside a variable temperature insert between 4.2 K and 77 K.
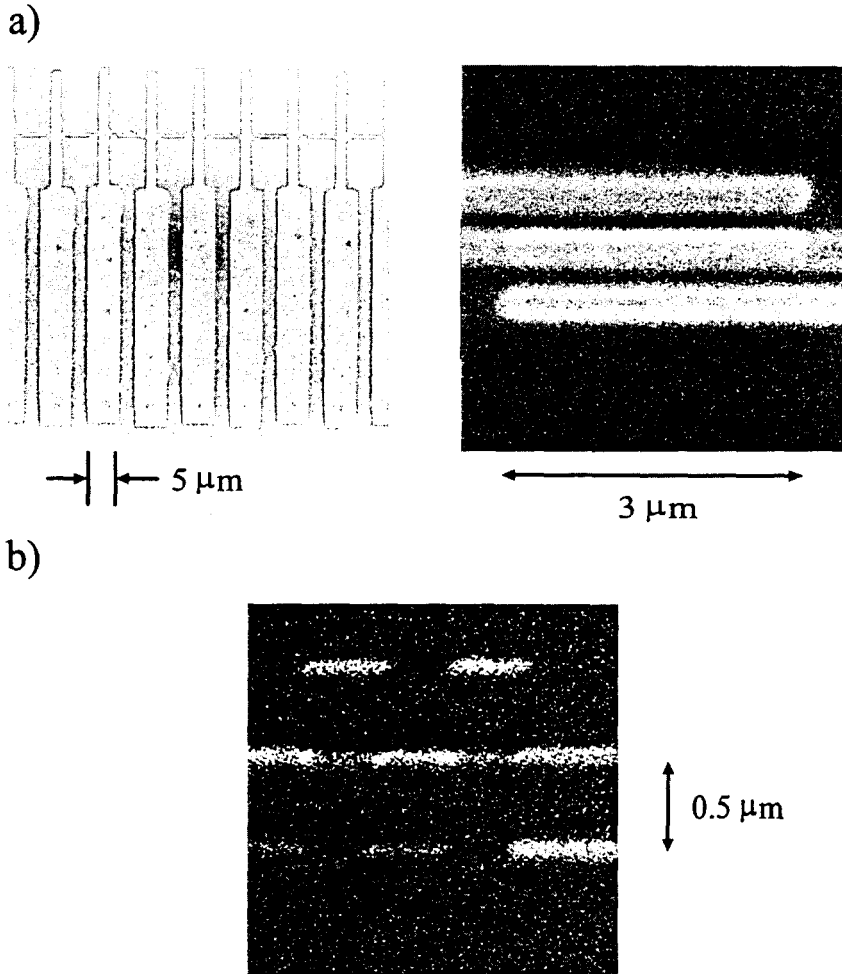
a)

→| |← 5 μm

◄————— 3 μm —————►

b)

↕ 0.5 μm

Fig. 4. Electron beam patterned aluminium based arrays of tunnel junctions for CBT thermometry. Array in (a) is for 50 mK $< T <$ 4 K, and array in (b) is for 1 K $< T <$ 50 K. Overlapping, brighter areas between the islands form the junctions in each case. Note that high temperature requires ultra small junctions, whereas low temperatures can be measured by large area junctions and islands.

4. EXPERIMENTAL RESULTS

A. Basic Results

Measured conductances follow the expression of Eq. (3) very closely. As an example we show in Fig. 5 data of a sample with $N = 20$ junctions at $T = 4.2$ K. The best fit to the data of Fig. 5 yields $V_{1/2} = 39.56$ mV, whereas the value calculated from Eq. (3) is 39.36 mV. In Fig. 6 we see data on the experimental N dependence of $V_{1/2}$ at $T = 4.2$ K for various samples with $\Delta G/G_T < 0.05$. The line has the theoretical slope $5.44 k_B T/e$ of Eq. (4). There is a slight deviation from the simple theoretical behaviour at low N, which we will discuss in Sec. 5. In Fig. 7 we show the experimental temperature dependence of (a) the width, $V_{1/2}$, and (b) the inverse height, $(\Delta G/G_T)^{-1}$ of a few samples with different values of N, together with $5.44 N k_B T/e$ by the solid line in (a). $V_{1/2}$ does not involve any fit parameters making our thermometer a primary one, whereas in (b) $\Delta G/G_T$ at one temperature gives u_N, whereby the rest of the line for each array is determined.

On the premise of the theoretical results in Sec. 2, our thermometer is self-calibrating, and thus primry, at any temperature. The two quantities, $V_{1/2}$ and $(\Delta G/G_T)^{-1}$, are fairly linear in T, respectively, over a wide temperature interval. The dynamic temperature range is determined on one hand by the signal to noise ratio to detect small changes of G at the high temperature end, and, on the other hand, by the approach of full Coulomb blockade at the low temperature end. By lock-in techniques we can
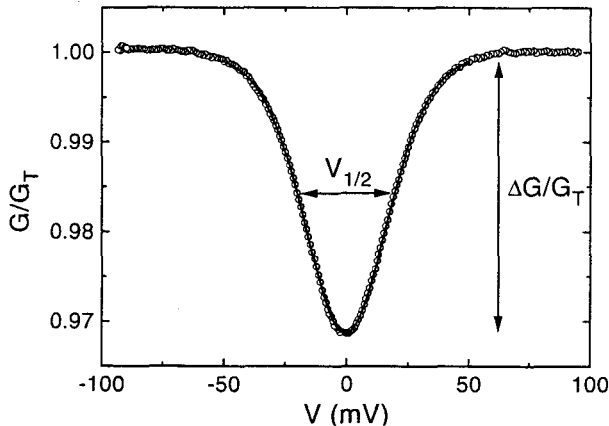

Fig. 5. An example of a measurement of an array of $N = 20$ junctions at $T = 4.2$ K. The solid line shows the analytical result by Eq. (3). Parameters $V_{1/2}$ and $\Delta G/G_T$ are introduced in the figure.
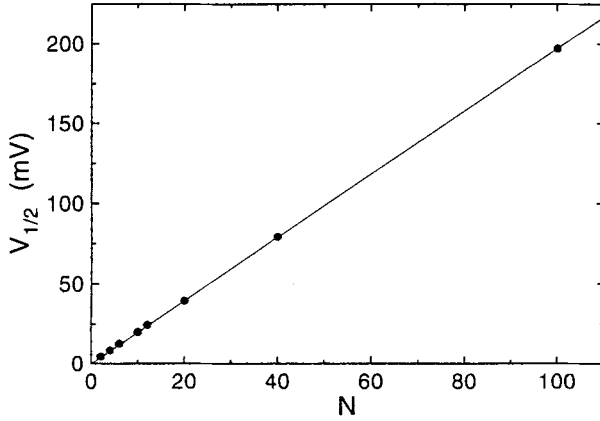
Fig. 6. Dependence of $V_{1/2}$ at $T = 4.21$ K on the number of junctions N in the array for a set of samples where $\Delta G/G_T \ll 1$. The straight line through the measured points corresponds to $V_{1/2} = 1.98$ mV $\times N$ by Eq. (4).

measure conductance minima with 5 % precision at $u_N \simeq 0.01$ ($\Delta G/G_T \simeq 0.2$ per cent) at the high temperature end, and the full Coulomb blockade limit is not yet approach when $u_N \simeq 1$. This gives the ratio of the maximum and the minimum measurable tempratures, $T_{max}/T_{min} \sim 100$, by just one array. The mean of the temperature range can be tailored by the size of the junctions, i.e., by u_N.
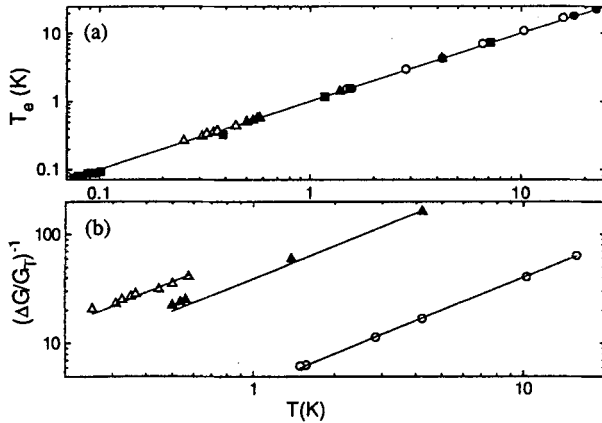

Fig. 7. The temperature dependence of (a) the width at half minimum, $V_{1/2}$, and (b) the inverse height, $(\Delta G/G_T)^{-1}$ of conductance curves of various samples. The solid line in (a) is form Eq. (3) and those in (b) are linear in T.

B. Tolerance to Magnetic Field

Low temperature thermometers insensitive to magnetic field are fairly rare[11]; Coulomb blockade might provide one. Features in Coulomb blockade should supposedly not depend on magnetic field when $E_F \gg \mu_B B$. This inequality is always satisfied in practice. Here, E_F is the Fermi energy of the metal, μ_B is the Bohr magneton and B is the magnetic flux density. Figure 8 shows measurements of magnetic field dependence of $V_{1/2}$ at three different temperatures. To within the 2% reproducibility of temperature no field dependence at any of the three temperatures of 4.2, 1.6, and 0.7 K can be observed. The only limitation as to magnetic field when using aluminium junctions seems to be the required suppression of superconductivity at $T < 1$ K.

C. Inhomogeneous Arrays

One of the more important factors affecting the applicability of junction arrays for precise measurements of absolute temperature is the tolerance of $V_{1/2}$ to inhomogeneities in the junction parameters as already discussed theoretically in Sec. 2. Figure 9 shows a set of measurements where arrays of varying deviations from a uniform chain were intentionally fabricated; experimental data are shown in open circles. The measurement
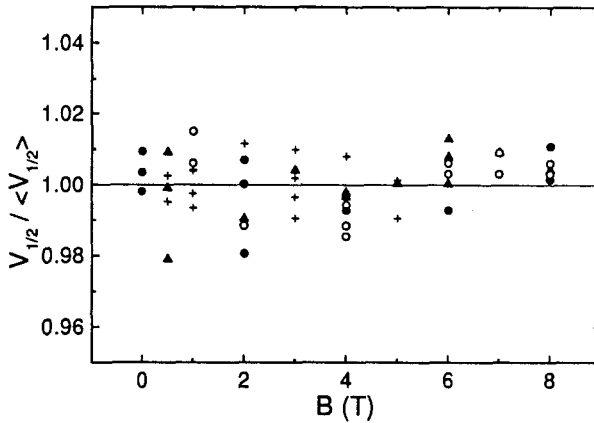

Fig. 8. Magnetic field dependence of $V_{1/2}$ divided by its mean value $\langle V_{1/2} \rangle$ within each set of data. The data are for $T = 4.2$ K, $N = 10$ (solid circles); $T = 1.6$ K, $N = 10$ (solid triangles); $T = 0.7$ K, $N = 10$ (open circles); and $T = 1.6$ K, $N = 40$ (crosses). The different values at the same field and with the same symbol reflect the scatter in measuring $V_{1/2}$. At $T = 0.7$ K a field of ~ 0.5 T was necessary to suppress superconductivity of aluminium.
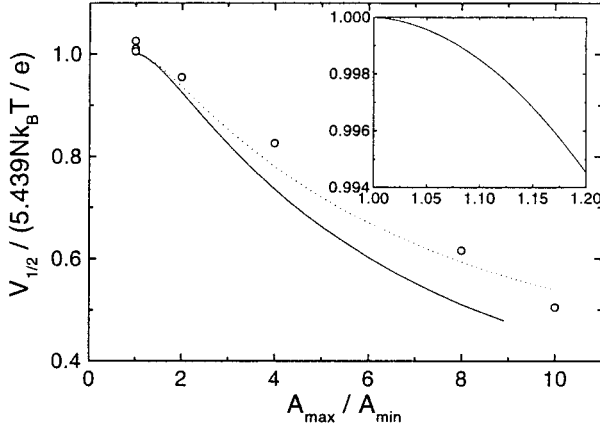
Fig. 9. The width of the conductance curve $V_{1/2}$, as scaled by the calculated width of a homogeneous array, $5.44Nk_BT/e$. The data in open circles represent experiments as a function of the width in the distribution of junction areas. For further definition of A_{max}/A_{min}, see text. The solid and dashed lines are the corresponding theoretical lines, with assumptions explained in the text. The inset with a solid line shows the magnification of the upper left hand corner, as given by Eq. (6).

was taken at $T = 4.2$ K with arrays where $\Delta G/G_T$ varied between 0.8% and 1.6%. A random type of distribution of junction areas in a chain of $N = 10$ was generated. All the chains possessed a similar distribution, but with a varying amplitude characterized by the parameter A_{max}/A_{min}, which is the ratio of the maximum and minimum areas of junctions within a chain. The geometrical width of each junction in the chain was nominally $0.2\ \mu$m, and, as an example, their lengths from one end of the chain to the other were 1, 1.4, 0.9, 1.1, 1.2, 0.75, 1, 1.3, 1.5, and $0.8\ \mu$m, respectively, for the case $A_{max}/A_{min} = 2$. Up to $A_{max}/A_{min} = 10$ we observe a drop of $V_{1/2}$ by a factor of two, at most, which already demonstrates weak dependence of this thermometric parameter on fabrication errors.

We may compare the experiment in Fig. 9 with the general high T expression of Eq. (1). Assuming uniform thickness of the aluminium oxide barrier throughout, we may suppose that $R_{T,i}C_i = constant$ for all junctions, because $R_{T,i} \propto A_i^{-1}$ and $C_i \propto A_i$, where A_i is the tunnelling area of junction i. Using this approximation and the distribution of junction parameters as set in the experimental layout we obtain the solid line in Fig. 9 in fair agreement with the experiment. We believe that the slight deviation is due to the fact that the real areas of the junctions deviate by a constant additional value from that of the lithographic pattern. The dashed line is the theoretical result assuming that there is an additional

area in each junction, which is 10% as compared to the area of the first one. An important conclusion involves the left hand upper corner of the figure, shown also by an inset, and given by Eq. (6). The numerical factor $k = 1.63$ for $N = 10$. In Fig. 9 this means that a 10% deviation, i.e., $A_{max}/A_{min} = 1.1$ induces a drop of 0.2% in $V_{1/2}$, only. With junction areas of nominally 0.2 μm^2 we can easily reach such a homogeneity, as supported by the small variation in the experimental values at $A_{max}/A_{min} = 1$ in Fig. 9.

D. Hot Electron Effects

Thermalisation of single electron devices is of considerable interest because of its fundamental and practical consequences. Heat transport between the conduction electrons and the lattice in a metal is believed to be well known and to obey a familiar $\propto T_e^5 - T_0^5$ law at low electron and lattice temperatures T_e and T_0, respectively. This law has been proven to be valid in thin films with uniform heating over a considerable surface area.[12-14] We have carried out an experimental investigation of the thermalisation of lithographically patterned tunnel junction arrays with thin film micron and submicron size metallic islands.[7] Such a study is vitally important, since in practical thermometry one is typically interested in the temperature of the surrounding lattice rather than the electronic system.

Consider a linear array of N tunnel junctions connected together by normal metal island electrodes. When biased at a voltage V across the ends of the chain, we have a power generated in junction i which equals $V^2 R_{T,i}/R_T^2$. This power is evenly shared by the two neighbouring islands. We have shown that this heat can hardly be transported away along the chain because of the high thermal resistance of the junctions, but it is, instead, leaking out from each island to the substrate via electron-phonon (el-ph) coupling and Kapitza resistance between the metal lattice and the silicon substrate, as depicted by the scheme in Fig. 10.

Assume an array perfectly thermalised at the (constant) temperature of the refrigerator at any bias voltage. If $u_N < 1$, Eq. (3) is very well obeyed in experiment by any symmetric array. Suppose this is not true due to either an extremely low temperature and/or insufficient volume and surface area of the island electrodes to thermalise. In this case the electronic temperature increases upon increasing bias due to the power dissipated. The shape of the conductance curve is thus distorted from that of Eq. (3).

We identify three island geometries in the following as: **A**—straight lines, 11×0.25 (μm)^2, connecting the junctions; **B**—an extension of 22×1.2 (μm)^2 added orthogonally to the geometry of **A**; **C**—an extension of 40×5 (μm)^2 further added to one end of the cooling fins of the geometry **B**.
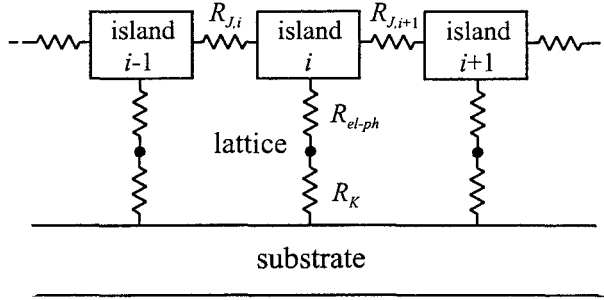
Fig. 10. A schematic thermal model of the array including the electronic thermal resistance of the junctions, $R_{J,i}$, the el-ph resistance, R_{el-ph}, and the Kapitza resistance to the substrate, R_K.

(The low T samples in Fig. 13a) are the type **C**.) The junctions in each case had a nominal overalp area of 0.25×3 $(\mu m)^2$.

Data of samples of types **A** and **C** are shown in Fig. 11 at $T = 200$ mK. Those of type **B** lie between these two extremes but they have been omitted for clarity. The solid line represents the analytic form of Eq. (3) with u_N
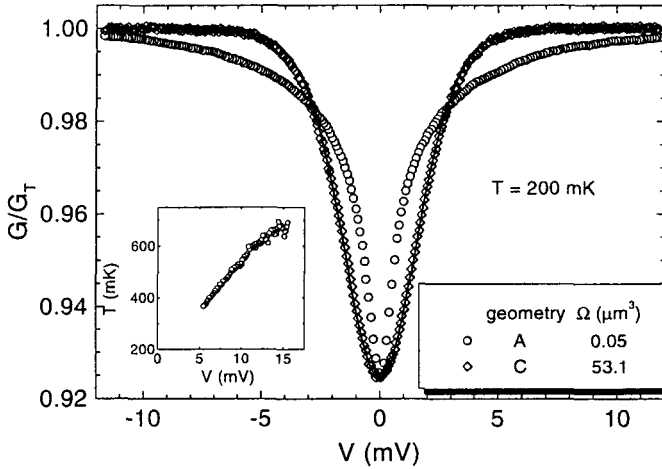

Fig. 11. Differential conductance G/G_T of two samples with $N = 40$ of types **A** and **C** at $T = 200$ mK. The values of $\varepsilon_c \equiv u_N k_B T$ for these samples are 0.090 K and 0.064 K, respectively. The corresponding volumes Ω are indicated for each sample in the figure. The dependence with constant temperature (Eq. (3)) is shown by the solid line. The depth of the drop of the sample of type **C** has been scaled by 1.42, to allow direct comparison between the two samples and the constant temperature model. The inset shows the dependence of the electronic temperature of the small sample (type **A**) as plotted against bias voltage.

parameter chosen to fit the experimental depth. The data of the sample with increased volume of the island closely follow the constant temperature curve but those of the array with small islands strongly deviate from this. We take this deviation as a quantitative measure of the thermal contact of the electrons on the islands to their surrounding lattice.

At low temperatures, where the shape of Eq. (3) is not anymore followed due to the heating by the bias current, we analysed the el-ph coupling at small temperature differences, i.e., near the minimum of the conductance dip. Assume first that the heating at zero bias is negligible, implying that $T_e = T_0$ at $V = 0$; in other words, we apply a sufficiently small AC-voltage to measure the differential conductance.

Secondly, we assume that heating on each island equals V^2/NR_T. Thirdly, the coupling between the electrons to the phonons is such that the power P of the heat transfer out of the electron system equals

$$P = \Sigma \Omega (T_e'' - T_0'') \tag{16}$$

where Ω is the volume of the electrode, and Σ and n are the parameters of coupling. Literatures gives $\Sigma \sim 1 \text{ nW/K}^5/(\mu\text{m})^3$ and $n = 5$ for uniform heating in a metal.[12][15] Using the three arguments above we obtain Σ and n for a given sample. Four typical examples are shown in Fig. 12 of samples of types **A** and **B** where $n = 5$ has been applied to find Σ as a function of T_0. We note that for the nonextended samples of type **A** the el-ph coupling
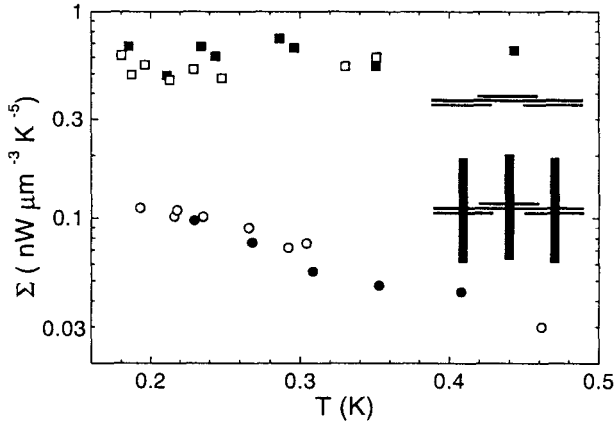

Fig. 12. Thermal contact parameter Σ obtained for four different samples using the conventional $n = 5$ power law. Squares, open and filled, are for non-extended islands of type **A** with film thicknesses 50 and 16 nm, respectively, whereas circles, open and filled, are for samples with extended islands of type **B** with film thickness of 13 nm in both cases.

can be presented in the form $P = \Sigma\Omega(T_e^5 - T_0^5)$, with $\Sigma \simeq 0.6 \text{ nW/K}^5/(\mu\text{m})^3$. This applies for both thin (16 nm) and thicker (50 nm) films, indicating that increasing the thickness, and thus volume, improves the thermal contact. For extended samples of type **B**, the contact is effectively weaker, and the dependence on T_0 is also weaker. The best fits in this in this case
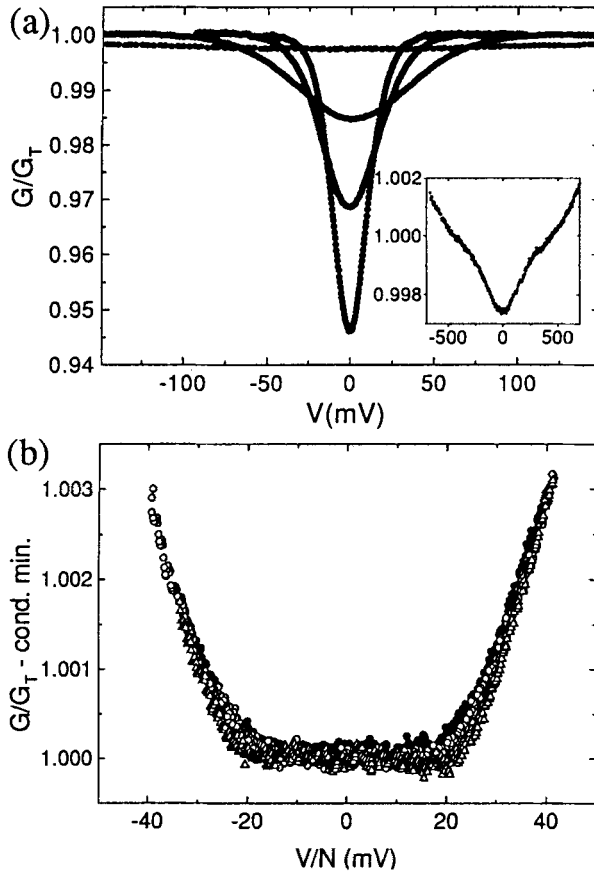

Fig. 13. (a) Differential conductance curves of a junction array (N = 20) as measured at various temperatures: 2.6, 4.2, 8.6 and 38 K. The lowest temperature corresponds to the deepest minimum. The inset shows the conductance measured at 38 K on a more proper scale (in the same units). (b) Conductances after the charging dips have been substracted. These sets of data were obtained by fitting the result of the Eq. (3) to the measured data with G_T, $V_{1/2}$ and $G(0)/G_T$ (or G_T, C and T) as adjustable parameters. Triangles are data measured at 25 K, whereas circles, filled and open, are measured at 38 and 43 K, respectively.

have $n \simeq 3.5$. Type C samples closely follow Eq. (3), i.e., they behave well for thermometry, and thus do not allow us to extract Σ.

The result of samples of type A agrees with the common expectation qualitatively and quantitatively. We are, however, unable to give a quantitative interpretation of the observation on the extended samples. We thus conclude that thermal coupling can be improved by increasing the volume of the island, but, upon increasing the surface area alone, the effective coupling constant is reduced possibly indicating the presence of local hot electrons.

E. High Temperature Limitations Due to Barrier Suppression

At the high temperature end CBT thermometry with aluminium based junctions is limited by the non infinite height of the tunnel barrier ($\simeq 2$ eV) of the insulating oxide layer between the electrodes. Because of this finite height the conductance depends on bias. This voltage dependence is present with no respect of charging effects. The Coulomb peak broadens and becomes lower toward higher temperatures and thus one cannot ultimately resolve this charging peak from the bias dependent background. We find agreement between the simple theory of Sec. 2 and measurements up to about 50 K, whereabove the effect due to the potential barrier becomes a dominating feature over the charging effect, unless the junctions are very small to enhance Coulomb blockade. Figure 13(a) shows conductance curves of a sample measured at various temperatures up to $T = 38$ K. We can see the influence of the barrier suppression in the highest temperature data, expanded in the inset.

Figure 13(b) shows differential conductance of the same array measured against bias voltage various temperatures. The charging minima have been numerically subtracted to allow straight comparison of the backgrounds. We can roughly estimate the maximum measurable temperature as follows. The charging peak is distinguishable from the background if the full width at half minimum, $V_{1/2}$, is less than half of the flat section of the background, which is 20 mV in Fig. 13(b). From Eq. (3) this gives roughly 40 K as the upper limit. Up to this temperature no corrections are needed. By subtracting the non linear background induced by the finite barrier we have been able to measure up to 77 K so far.

5. SHORT ARRAYS AND SOLITARY JUNCTIONS

Unlike arrays, a solitary tunnel junction is believed to show no charging effects in the simplest picture with perfect voltage bias across. Experimentally, a significant zero bias anomaly in the form of a drop of

conductance exists also in single junctions.[16-19] This is reflected by our data in Fig. 14(a), where the normalised conductance, G/G_T, against bias voltage V at high temperature ($T = 4.2$ K) is shown for a set of samples with $N = 1$, 2, 4 and 8 junctions in series separated by 3 μm long islands. The insets show the values of $V_{1/2}$ and $\Delta G/G_T$ for these data. One would not expect such a smooth dependence on N down to $N = 1$ in case the single junction peak would arise from a totally different origin as opposed to the case of $N > 1$. We can explain this behavior if we assume that the dominating capacitance determining the charging anomaly is that of the junction and not the environment.

Let us first discuss the IV characteristics of a solitary tunnel junction in the general case with capacitances C_{e1} and C_{e2} at this terminals (Fig. 14(b)).
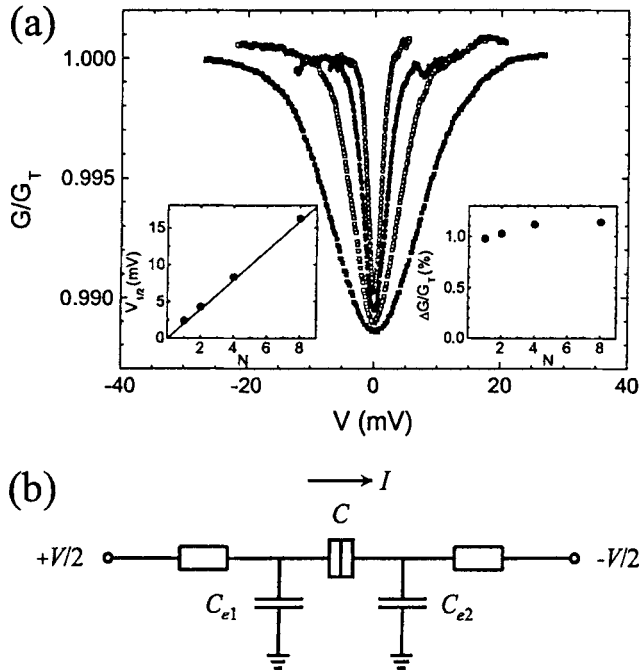

Fig. 14. (a) Differential conductance scaled by its asymptotic value at $eV \gg k_B T$ of various samples with identical tunnel junctions fabricated in one batch. The data are for different lengths, N, of arrays: circles, $N = 1$; solid circles, $N = 2$; squares, $N = 4$; filled squares, $N = 8$. The measurement was taken at $T = 4.2$ K. The insets show $V_{1/2}$ and $\Delta G/G_T$ of these data against N together with the theoretical "thermometer formula": $eV_{1/2} \simeq 5.44 N k_B T$ shown by a continuous line. Note that the depth is practically constant down to $N = 1$. (b) A schematic representation of a single junction including the environment with capacitances C_{ei}.

These two capacitances arise from the sections of electrodes attached to the junction, contributing to the charging energy, and this way they define the so called "horizon." Suppose that the bias across the junction equals V prior to the tunnelling event. Due to the shortness of the tunnelling time and the remoteness of the voltage source we may assume that the bias across the junction drops at the very instant of the electron tunnelling event by an amount $\Delta V = e/(C + C_e/2)$, and we set $C_{e2} = C_{e1} \equiv C_e$ for simplicity. This drop and the initial bias determine the two tunnelling rates in the forward and backward directions, respectively. Denoting $v_x = eV/k_B T$ and $u_x = (e^2/C_{eff})/k_B T$, we obtain a similar result as for the arrays (Eq. (3)), but now for $N = 1$: The differential conductance scaled by its asymptotic values at large V, G/G_T, reads

$$G/G_T = 1 - u_x g(v_x) \tag{17}$$

in a linear expansion in u_x, i.e., at high temperature. The depth of the conductance dip, $\Delta G/G_T$, is given by $\Delta G/G_T = u_x/6$. Furthermore, its full width at half minimum, $V_{1/2}$, is $V_{1/2} \simeq 5.44 k_B T/e$.

We can treat this problem also directly based on the microscopic theory reviewed in Ref. 20. From this theory we obtain an equation for tunnelling rates, which can be written as

$$\Gamma^{\pm}(V) = \frac{1}{e^2 R_T} \int_{-\infty}^{\infty} \gamma(\pm eV - E) \, P(E) \, dE \tag{18}$$

where $\gamma(x) = x/(1 - \exp(-x/k_B T))$, and $P(E)$ is the probability for an electron to exchange energy E with the environment in a tunnelling event. The current can now be calculated from $I = e[\Gamma^+(V) - \Gamma^-(V)]$.

Because $P(E)$ is peaked around $E = 0$ and vanishes as E tends to $\pm\infty$, we can expand the $\gamma(\pm eV - E)$ around $\pm eV$. By substituting this expansion to the formulae of current up to the first order and using the facts that $\int P(E) \, dE = 1$ and $\int EP(E) \, dE = e^2/2C$ we obtain Eq. (17) again. This result also explains the conductance curves in Fig. 14(a), in particular for $N = 1$.

Upon lowering T, C_{eff} increases, and the single junction peak becomes practically negligible. This behaviour is very interesting fundamentally, and important for the accuracy of the CBT thermometers with short arrays. To be a bit more specific, let us find a proper distance of the horizon. We adopt the idea that there is an uncertainty time for tunnelling, τ, given by $\tau \sim \hbar/\Delta E$ with $\Delta E < max(eV, k_B T)$[15,21]; this gives a consistent time scale with the environment theory[20] but we would like to stress that uncertainty time τ defined here is not the traversal time of tunnelling nor the uncertainty time associated with the Coulomb energy. We take $\ell \sim c\tau$, where c

is the propagation velocity of the electromagnetic signals. At zero bias ($V=0$), with $\Delta E = k_B T$, this yields a geometrical relation

$$C_c = c_L \ell \sim c_L c\tau \sim c_L c\hbar / k_B T \tag{19}$$

where c_L is the capacitance per unit length of the conductor strip attached to the junction given by $c_L = 2\pi\varepsilon_0\varepsilon_{eff}/\ln(8d/w)$, where ε_{eff} is the effective dielectric constant of the surrounding medium, d is the distance to the ground conductor, and w is the width of the strip. For a typical strip of $w \simeq 1\,\mu$m, $d \simeq 1$ mm, and $\varepsilon_{eff} \simeq 5$,[19] we obtain $c_L \simeq 3\cdot 10^{-11}$ F/m. C_c drops as T^{-1}, and ultimately it is just the geometrical junction capasitance C that determines the voltage drop $\Delta V = e/C$ at high enough T. Using the relation $\Delta G/G_T = u_s/6$ we find

$$(\Delta G/G_T)^{-1} = 6/u_s = 6(C + C_c/2)k_B T/e^2 \tag{20}$$

and combining this with Eq. (18) we finally obtain

$$(\Delta G/G_T)^{-1} = 6Ck_B T/e^2 + \delta \tag{21}$$

i.e., the inverse of height is linear in T (and C), but has a positive offset of

$$\delta \sim 3c_L c\hbar/e^2 \tag{22}$$

due to the simultaneous decrease of charging and thermal energies upon cooling. This effect is beautifully demonstrated by the data in Fig. 15 where a well developed $\delta \simeq 15 \ldots 20$ can be observed as an offset in both (a) and (b).

A particularly clean environment of a single junction can be realised in experiment by nanoscale on chip resistors using a multiple angle shadow evaporation technique. In the first experiment we applied two thin film chromium resistors of 100 nm linewidth and $3\,\mu$m length symmetrically at a distance of $1\,\mu$m from the junction producing resistances of about 1.5 kΩ each. The environment, unlike in the case of nonresistively connected solitary junctions, is now more spatially restricted, and the charging effects at low temperatures are enhanced due to a small effective capacitance.

Figure 16 shows data taken of such a resistively surrounded single junction. This preliminary measurement was realised just in a simple two wire configuration, thus not discriminating between voltage drops, or resistances, of the chromium resistors and the junction itself. The junction resistance was, however, about 60 kΩ, i.e., more than an order of magnitude higher than that of the Cr leads, and the voltage drop in Fig. 16 thus represents mostly that across the junction, and only about 5 % across
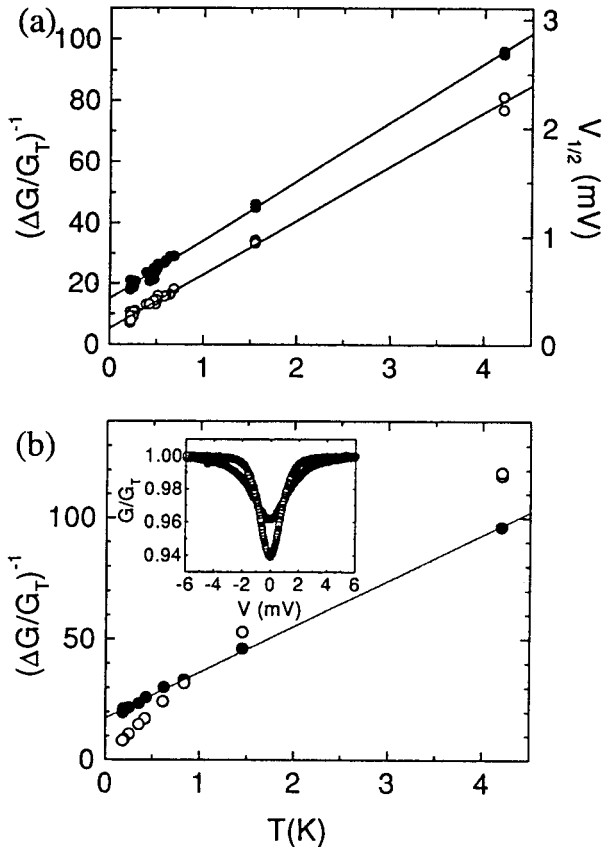
Fig. 15. (a) Temperature dependences of both $V_{1/2}$ (circles) and $(\Delta G/G_T)^{-1}$ (filled circles) as measured for a single junction with $R_T = 55$ kΩ and $A = 0.28$ $(\mu m)^2$. Both the quantities are linear in T but both of them, $(\Delta G/G_T)^{-1}$ in particular, have a positive offset. To compare the temperature dependence of single junctions as opposed to one dimensional arrays with small islands in between the junctions, we show in Fig. (b) data of a series connection of eight single junctions with large contact pads of 500×500 $(\mu m)^2$ in between, together with results on a one dimensional array of eight tunnel junctions with 10 μm long islands in between. In the two samples, fabricated within the same batch, all the 16 junctions were identical to within $\sim 10\%$ in R_T or A. The offset of the "single junction" sample is close to that in (a) but the data of the eight junction chain behaves in a different way: the dependence is nonlinear because there is a crossover from the environment dominated behaviour at low temperatures to the junction dominated behaviour at higher temperatures. Because of a small islands the charging energy does not vanish even at low T and the data set threads through origin without offset in this case. The inset shows the differential conductance of the two samples against bias at $T \simeq 0.5$ K. In each case the average value of R_T was about 28 kΩ.
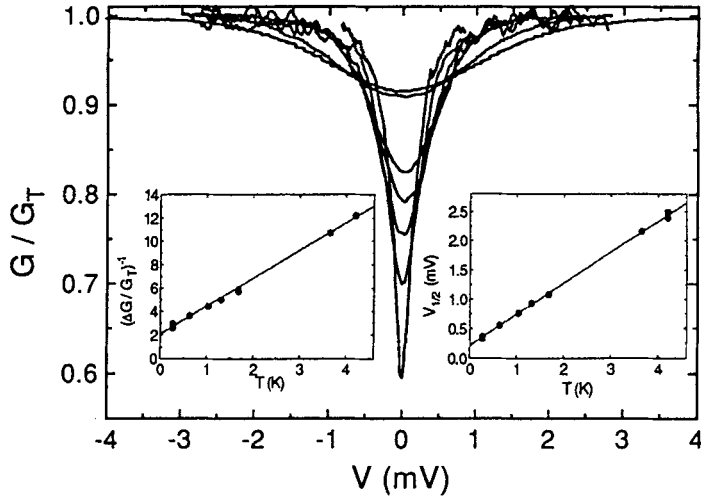
Fig. 16. Data of a single junction with $R_T \simeq 60 \, k\Omega$ and an area of about $0.2 \, \mu m \times 0.1 \, \mu m$, in a resistive environment ($R_e \simeq 3 \, k\Omega$). The main figure displays the conductance dip against bias voltage across the resistors and the junction in series, at various temperatures in the range of 0.2 K–4. K. The insets show the corresponding inverse depth on the left, and the half width on the right as functions of temperature. The solid lines are linear fits to the data.

the environment. The data display two drastic, although well expected, differences from those of the solitary nonresistively coupled single junctions. Firstly, the conductance dip is at all temperatures deeper than in the earlier measurements, reaching almost 50% at the lowest temperatures, in contrast to 5% of the nonresistively configured junctions, in accordance with the idea of local charging at the site of the junction. Secondly, which in fact is related to the first feature, the width of the peak is closer to being proportional to T than in the earlier measurements. This can also be understood with the model of a spatially restricted capacitor.

6. SUMMARY

In this article we have reviewed the use of tunnel junction arrays for primary thermometry which is based on the main result of Eq. 4 which shows that the half width of the conductance dip at zero bias, $V_{1/2,0}$, measured in an array, is proportional to temperature. Since the proportionality constant is determined by just the fundamental constants e and k_B and N, the number of junctions in the array, it is evident that the thermometer is primary. Also the depth of the conductance dip, $\Delta G/G_T$, can be used as a secondary thermometer.

A new important result of this article is the linear correction to the half width $V_{1/2,0}$, shown in Eq. 13, which is needed in the low temperature regime; this temperature range is specific to each array. The correction arises from the higher order terms in the high temperature expansion used. We also obtain a similar correction to the depth of the conductance dip, and it is shown in Eq. 14.

In practice, according to our experiments and calculations, the tunnel junction arrays can presently be used as a thermometer from a few mK up to about 77 K, using arrays of different sizes. The low temperature limit is due to the poor electron phonon coupling down there, which was discussed in Sec. 4D. The upper limit is brought about by the non infinite height of the tunnel barrier of aluminium based junctions (Sec. 4E).

Experimentally, the CBT thermometer is insensitive to changes in the magnetic field and, what is fundamental to its operation in contrast to conventional single electron devices, it is also immune to the ever present fluctuations of the background charges. Inhomogenities in the array yield, however, a small quadratic correction to $V_{1/2}$, given by Eq. 15. This dependence is nevertheless quite weak in standard arrays fabricated by electron beam lithography (Ch. 3).

An interesting observation is that short arrays, single tunnel junctions in particular, show interesting deviations from the universal behaviour of the long arrays discussed above. This is due to the frequency dependent impedance of the connecting wires within what is often called a "horizon" of the junction. The distance of the horizon is determined by the uncertainty time for tunnelling τ, determined by $h/\Delta E$ with $\Delta E = max(eV, k_B T)$. The problem can also be treated based on the microscopic theory reviewed in Ref. 20, which yields in our case the same result as the phenomenological horizon model. This behaviour of single tunnel junctions causes end effects in long arrays. However, their influence can be suppressed by increasing the number of junctions in the array.

More detailed studies of certain aspects of our work have been reported earlier in Refs. 4, 5, 6, 7 and 8.

ACKNOWLEDGMENTS

REFERENCES

1. D. V. Averin and K. K. Likharev, in *Mesoscopic Phenomena in Solids*, B. L. Altshuler, P. A. Lee, and R. A. Webb (eds.), Elsevier, Amsterdam (1991).

2. P. Delsing, in *Single Charge Tunneling, Coulomb Blockade Phenomena in Nanostructures*, H. Grabert and M. H. Devoret (eds.), Plenum Press, New York (1992), p. 249.
3. M. H. Devoret and H. Grabert, *ibid.*, p. 1.
4. J. P. Pekola, K. P. Hirvi, J. P. Kauppinen, and M. A. Paalanen, *Phys. Rev. Lett.* **73**, 2903 (1994).
5. K. P. Hirvi, J. P. Kauppinen, A. N. Korotkov, M. A. Paalanen, and J. P. Pekola, *Appl. Phys. Lett.* **67**, 2096 (1995).
6. K. P. Hirvi, M. A. Paalanen, and J. P. Pekola, *J. Appl. Phys.* **80**, 256 (1996).
7. J. P. Kauppinen and J. P. Pekola, *Phys. Rev. B* **54**, R8353 (1996).
8. J. P. Kauppinen and J. P. Pekola, *Phys. Rev. Lett.* **77**, 3889 (1996).
9. N. S. Bakhvalov, G. S. Kazacha, K. K. Likharev, and S. I. Serdyukova, *Sov. Phys. JETP* **68**, 581 (1989) [*Zh. Eksp. Teor. Fiz.* **95**, 1010 (1989)].
10. J. P. Pekola and J. P. Kauppinen, *Cryogenics* **34**, 843 (1994).
11. See, e.g., F. Pobell, *Matter and Methods at Low Temperatures*, Springer Verlag, Berlin Heidelberg (1992).
12. M. L. Roukes, M. R. Freeman, R. S. Germain, R. C. Richardson, and M. B. Ketchen, *Phys. Rev. Lett.* **55**, 422 (1985).
13. F. C. Wellstood, C. Urbina, and J. Clarke, *Appl. Phys. Lett.* **54**, 2599 (1989).
14. F. C. Wellstood, C. Urbina, and J. Clarke, *Phys. Rev. B* **49**, 5942 (1994).
15. R. L. Kautz, G. Zimmerli, and J. M. Martinis, *J. Appl. Phys.* **73**, 2386 (1993).
16. L. J. Geerligs, V. F. Anderegg, C. A. van der Jeugd, J. Romijn, and J. E. Mooij, *Europhys. Lett.* **10**, 79 (1989).
17. P. Delsing, K. K. Likharev, L. S. Kuzmin, and T. Claeson, *Phys. Rev. Lett.* **63**, 1180 (1989).
18. A. N. Cleland, J. M. Schmidt, and J. Clarke, *Phys. Rev. Lett.* **64**, 1565 (1990).
19. P. Wahlgren, P. Delsing, and D. B. Haviland, *Phys. Rev. B* **52**, 2293 (1995); P. Wahlgren, licentiate thesis, Chalmers University of Technology (1995).
20. G.-L. Ingold and Yu. V. Nazarov, in *Single Charge Tunneling, Coulomb Blockade Phenomena in Nanostructures*, H. Grabert and M. H. Devoret (eds.), Plenum Press, New York (1992), p. 21.
21. Yu. V. Nazarov, *Zh. Eksp. Teor. Fiz.* **95**, 975 (1989) [*Sov. Phys. JETP* **68**, 561 (1989)].